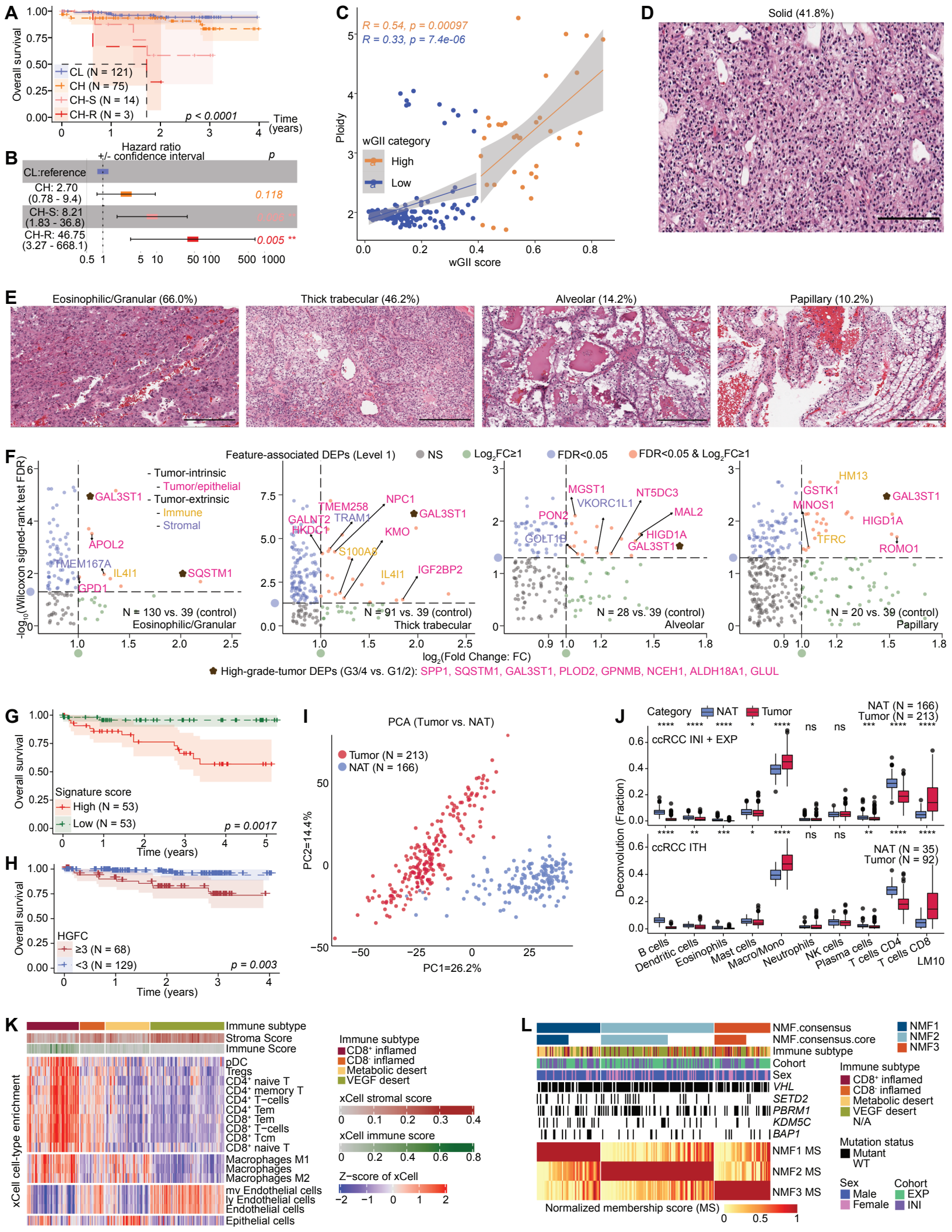
A
Overall survival
CL (N = 121)
CH (N = 75)
CH-S (N = 14)
CH-R (N = 3)
p < 0.0001
Time (years)
B
Hazard ratio
+/- confidence interval
p
CL:reference
CH: 2.70 (0.78 - 9.4)
0.118
CH-S: 8.21 (1.83 - 36.8)
0.006 **
CH-R: 46.75 (3.27 - 668.1)
0.005 **
C
R = 0.54, p = 0.00097
R = 0.33, p = 7.4e-06
Ploidy
wGII category
High
Low
wGII score
D
Solid (41.8%)
E
Eosinophilic/Granular (66.0%)
Thick trabecular (46.2%)
Alveolar (14.2%)
Papillary (10.2%)
F
Feature-associated DEPs (Level 1)
NS
Log2FC≥1
FDR<0.05
FDR<0.05 & Log2FC≥1
- Tumor-intrinsic
- Tumor/epithelial
- Tumor-extrinsic
- Immune
- Stromal
-log10(Wilcoxon signed-rank test FDR)
GAL3ST1
APOL2
TMEM167A
IL4I1
SQSTM1
GPD1
N = 130 vs. 39 (control)
Eosinophilic/Granular
TMEM258
NPC1
GALNT2
TRAM1
FKDC1
KMO
S100A8
IL4I1
IGF2BP2
N = 91 vs. 39 (control)
Thick trabecular
MGST1
VKORC1L1
NT5DC3
PON2
MAL2
GOLT1B
HIGD1A
N = 28 vs. 39 (control)
Alveolar
HM13
GSTK1
MINOS1
HIGD1A
TFRC
ROMO1
N = 20 vs. 39 (control)
Papillary
log2(Fold Change: FC)
High-grade-tumor DEPs (G3/4 vs. G1/2): SPP1, SQSTM1, GAL3ST1, PLOD2, GPNMB, NCEH1, ALDH18A1, GLUL
G
Overall survival
Signature score
High (N = 53)
Low (N = 53)
p = 0.0017
Time (years)
H
Overall survival
HGFC
≥3 (N = 68)
<3 (N = 129)
p = 0.003
Time (years)
I
PCA (Tumor vs. NAT)
Tumor (N = 213)
NAT (N = 166)
PC2=14.4%
PC1=26.2%
J
Category
NAT
Tumor
NAT (N = 166)
Tumor (N = 213)
ccRCC INI + EXP
ccRCC ITH
NAT (N = 35)
Tumor (N = 92)
Deconvolution (Fraction)
B cells
Dendritic cells
Eosinophils
Mast cells
Macro/Mono
Neutrophils
NK cells
Plasma cells
T cells CD4
T cells CD8
LM10
K
Immune subtype
Stroma Score
Immune Score
xCell cell-type enrichment
pDC
Tregs
CD4+ naive T
CD4+ memory T
CD4+ T−cells
CD4+ Tem
CD8+ Tem
CD8+ T−cells
CD8+ Tcm
CD8+ naive T
Macrophages M1
Macrophages
Macrophages M2
mv Endothelial cells
ly Endothelial cells
Endothelial cells
Epithelial cells
Immune subtype
CD8+ inflamed
CD8- inflamed
Metabolic desert
VEGF desert
xCell stromal score
xCell immune score
Z−score of xCell
L
NMF.consensus
NMF.consensus.core
Immune subtype
Cohort
Sex
VHL
SETD2
PBRM1
KDM5C
BAP1
NMF1 MS
NMF2 MS
NMF3 MS
Normalized membership score (MS)
NMF1
NMF2
NMF3
Immune subtype
CD8+ inflamed
CD8- inflamed
Metabolic desert
VEGF desert
N/A
Mutation status
Mutant
WT
Sex
Male
Female
Cohort
EXP
INI

Figure S1. Association between high-grade feature count (HGFC) and overall survival, immune and multi-omic clusters, related to Figure 1.

A) Overall survival difference among the four histopathologic subtypes indicated by Kaplan Meier plot indicates the association between overall survival and histopathologic subtypes. Log-rank test $p < 0.0001$.

B) The hazard ratios of the histopathologic subtypes CH, CH-S, and CH-R compared to the CL reference. Cox proportional hazards model p is calculated. Whiskers represent + / - 95% confidence intervals of the hazard ratios.

C) Scatter plot shows the correlation between the wGII score and ploidy values of all the tumor samples. Tumors were grouped as either containing high or low wGII values. Correlation test p was calculated. R represents Pearson correlation coefficient.

D & E) Representative H&E showing the seven high-grade features in schema: solid, eosinophilic/granular change, thick trabeculae, alveolar, and papillary/pseudopapillary pattern, respectively. Scale bar = 200 microns.

F) Proteomic changes associated with tumor architecture (pattern) and cytology subtypes. Volcano plots showed DEPs associated with certain high-grade features. They were identified from DE analysis by comparing such tumors with controls (tumors without any of the seven high-grade features, N = 39). Using snRNA-seq, we distinguished the expression profiles of these markers in different cell populations (three major categories: tumor epithelial, immune, and stroma) and labeled the markers by different colors. We performed DE analysis on multiple levels: (bulk proteogenomic expression / snRNA-seq) x (cohort / case / segment / tumor-sub-cluster level). Here is Level 1 DE analysis: bulk DEGs/DEPs on the cohort level. DEPs associated with high-grade are listed at the bottom for comparison. FDR indicates false discovery rate.

G) Kaplan Meier plot shows the association between integrative signature score (based on protein abundance of LRRC5, RPN2, and SERPINH1 weighted by length) and overall survival (cases divided into the upper quartile and lower quartile for comparison). Log-rank test p is 0.0017. The hazard ratio of high group is 4.10 (1.01 - 16.8) from Cox model ($p = 0.049$).

H) Kaplan Meier plot shows the association between HGFC and overall survival (cases divided into those containing less than 3 or 3 and above HGFC features). Log-rank test p is 0.003. The hazard ratio of ≥3 group is 3.70 (1.07 - 12.8) from Cox model ($p = 0.039$).

I) Principal component analysis (PCA) of proteomics data obtained from tumors (red dots) and normal adjacent tissues (NATs, blue dots).

J) Box plots representing immune cell type (10 different cell types) abundance as assessed by CIBERSORTx deconvolution tool using Leukocyte signature Matrix 10 (LM10). The comparison of bulk deconvolution with LM10 between tumors (red) and NATs (blue) in INI and EXP cohorts (top panel) and ITH cohort (bottom panel) are shown (Asterix represents significance; ns- not significant). Wilcoxon signed-rank test p is calculated. ns $p > 0.05$, * $p \leq 0.05$, ** $p \leq 0.01$, *** $p \leq 0.001$, **** $p \leq 0.0001$. Boxes represent the interquartile range (IQR, e.g., median indicated by solid line in box, 0.25 and 0.75 quantiles) and whiskers represent the largest and smallest values within 1.5 x IQR range.

K) Heatmap represents the xCell cell-type-enrichment-based immune subtyping performed for the entire cohort. The four immune subtypes identified include $CD8^+$ inflamed; $CD8^-$ inflamed; metabolic desert; and VEGF desert as represented in the first track. Stroma, immune scores, and enrichment signatures noted for representative cell types are presented below (e.g., ly Endothelial cells: Lymphatic endothelial cells; mv Endothelial cells: Microvascular endothelial cells).

L) Multi-omic subtyping based on non-negative matrix factorization (NMF). RNA expression, CNV, and global protein abundance data were integrated into this analysis to reveal NMF sample clusters contained in this cohort. The bottom part of the heatmap indicated the membership score of each subtype.

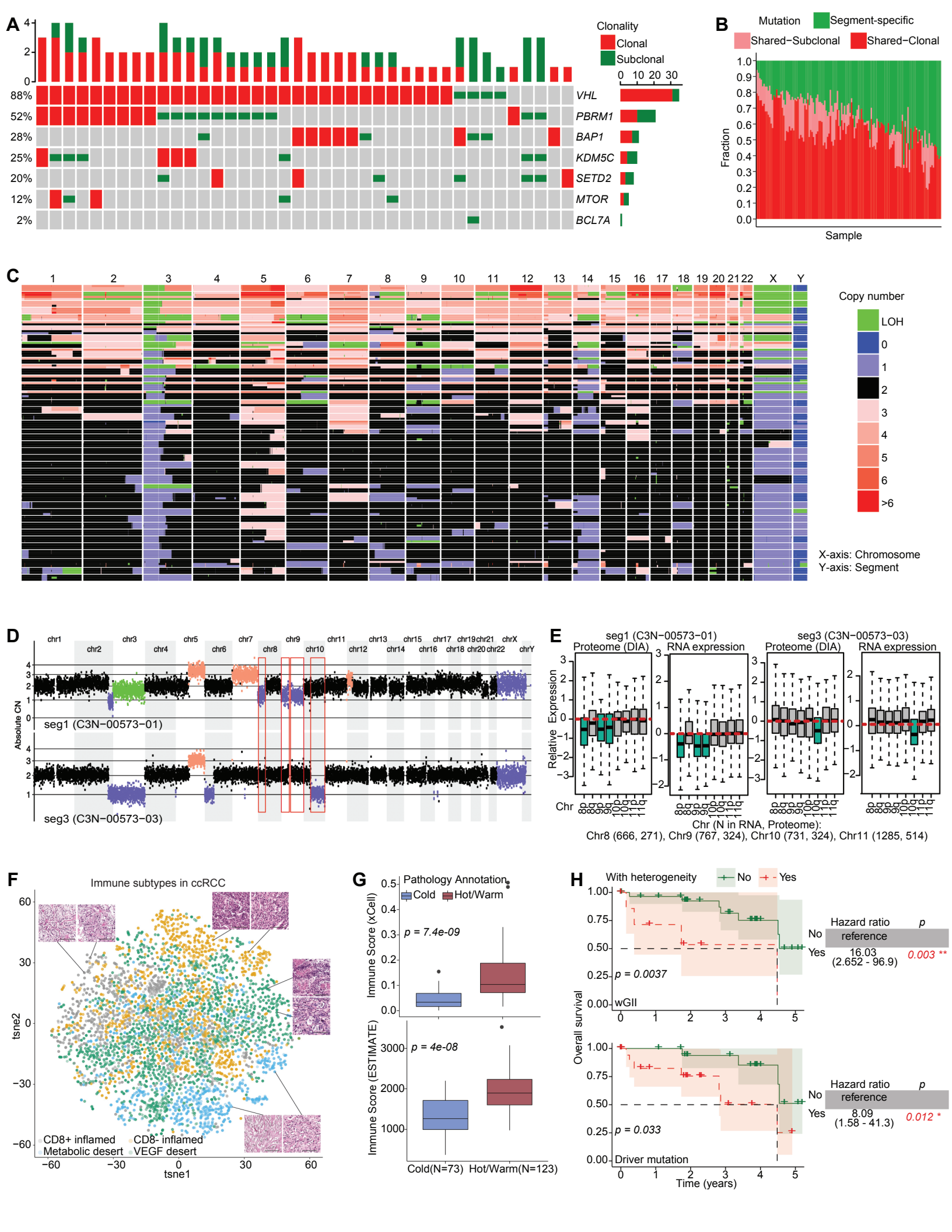
A
Clonality
Clonal
Subclonal
0 10 20 30
88% VHL
52% PBRM1
28% BAP1
25% KDM5C
20% SETD2
12% MTOR
2% BCL7A
B
Mutation
Segment-specific
Shared−Subclonal
Shared−Clonal
Fraction
Sample
C
Copy number
LOH
0
1
2
3
4
5
6
>6
X-axis: Chromosome
Y-axis: Segment
D
Absolute CN
seg1 (C3N−00573−01)
seg3 (C3N−00573−03)
E
seg1 (C3N−00573−01)
seg3 (C3N−00573−03)
Proteome (DIA)
RNA expression
Relative Expression
Chr
Chr (N in RNA, Proteome):
Chr8 (666, 271), Chr9 (767, 324), Chr10 (731, 324), Chr11 (1285, 514)
F
Immune subtypes in ccRCC
CD8+ inflamed
CD8- inflamed
Metabolic desert
VEGF desert
tsne1
tsne2
G
Pathology Annotation
Cold
Hot/Warm
p = 7.4e-09
Immune Score (xCell)
p = 4e-08
Immune Score (ESTIMATE)
Cold(N=73)
Hot/Warm(N=123)
H
With heterogeneity
No
Yes
p = 0.0037
wGII
Hazard ratio
p
reference
16.03
(2.652 - 96.9)
0.003 **
p = 0.033
Driver mutation
8.09
(1.58 - 41.3)
0.012 *
Overall survival
Time (years)

Figure S2. Integrated proteogenomic analysis of ccRCC genetic and TME heterogeneity, related to Figure 2.

A) Landscape of driver mutations and their clonality across the ITH cohort segments. Each column represents all segments from a given case. While VHL aberrations were predominantly clonal (red) in nature, others showed greater degrees of sub-clonality (green).

B) Heatmap depicts the frequency of segment-specific (green), shared-subclonal (pink), and shared-clonal (red) somatic mutational events found across tumors and/or even across segments of a given tumor.

C) Heatmap of the absolute copy number determined from whole exome / whole genome sequencing data for 132 tumor segments obtained from 40 ccRCC patients in the ITH cohort (cases clustered by CNV pattern and segments ordered by case numbers. Each row (x-axis) depicts a segment from a given case and columns (y-axis) represent chromosomes. Black: diploid; green: loss of heterozygosity; blue: copy loss; red: copy gains. CNV heterogeneities (e.g., chr5, 7, 9, 14) indicate the varied tumor subpopulations.

D) Absolute copy number (CN) plots reveal the copy number heterogeneity found across segments for a given case (C3N−00573). Black: diploid; green: loss of heterozygosity; blue: copy loss; and red: copy gains. Red boxes highlight the observed copy number losses on chromosomes 8, 9, and 10.

E) Dosage effects of CNV observed at protein and RNA expression levels. Box plots show the relative expression (tumor vs. normal) of genes and proteins found on chromosomes 8, 9, and 10 for the two segments from case C3N-00573. Corresponding loss of expression (green) associated with copy number change can be readily visualized as compared to genes on unaltered chromosomes (Gray) in each segment. Boxes represent the interquartile range (IQR, e.g., median indicated by solid line in box, 0.25 and 0.75 quantiles) and whiskers represent the largest and smallest values within 1.5 x IQR range.

F) t-SNE of the data obtained from Panoptes-based multi-resolution neural network models that were trained to predict immune subtypes based on H&E images. Each dot represents a tile from a sample with dots colored by the immune subtypes, representing specific tiled regions on H&E images. Scale bar = 200 microns.

G) High concordance was observed between the sample immune annotations rendered by pathology team review and by data-driven delineation for the overall immune infiltration level (ESTIMATE immune score and xCell immune score). Wilcoxon signed-rank test p is calculated. Boxes represent the interquartile range (IQR, e.g., median indicated by solid line in box, 0.25 and 0.75 quantiles) and whiskers represent the largest and smallest values within 1.5 x IQR range.

H) Overall survival difference among the cases with vs. without heterogeneity in wGII status or driver mutations (in *VHL, PBRM1, KDM5C, SETD2, BAP1*). Kaplan Meier plot indicates the association between overall survival and wGII or driver mutation heterogeneity. Forest plot for Cox Proportional Hazards Model shows the hazard ratio by adjusting by age, sex, and tumor grade. Log-rank test p is calculated. Cox model hazard ratio is shown in the table on the right.

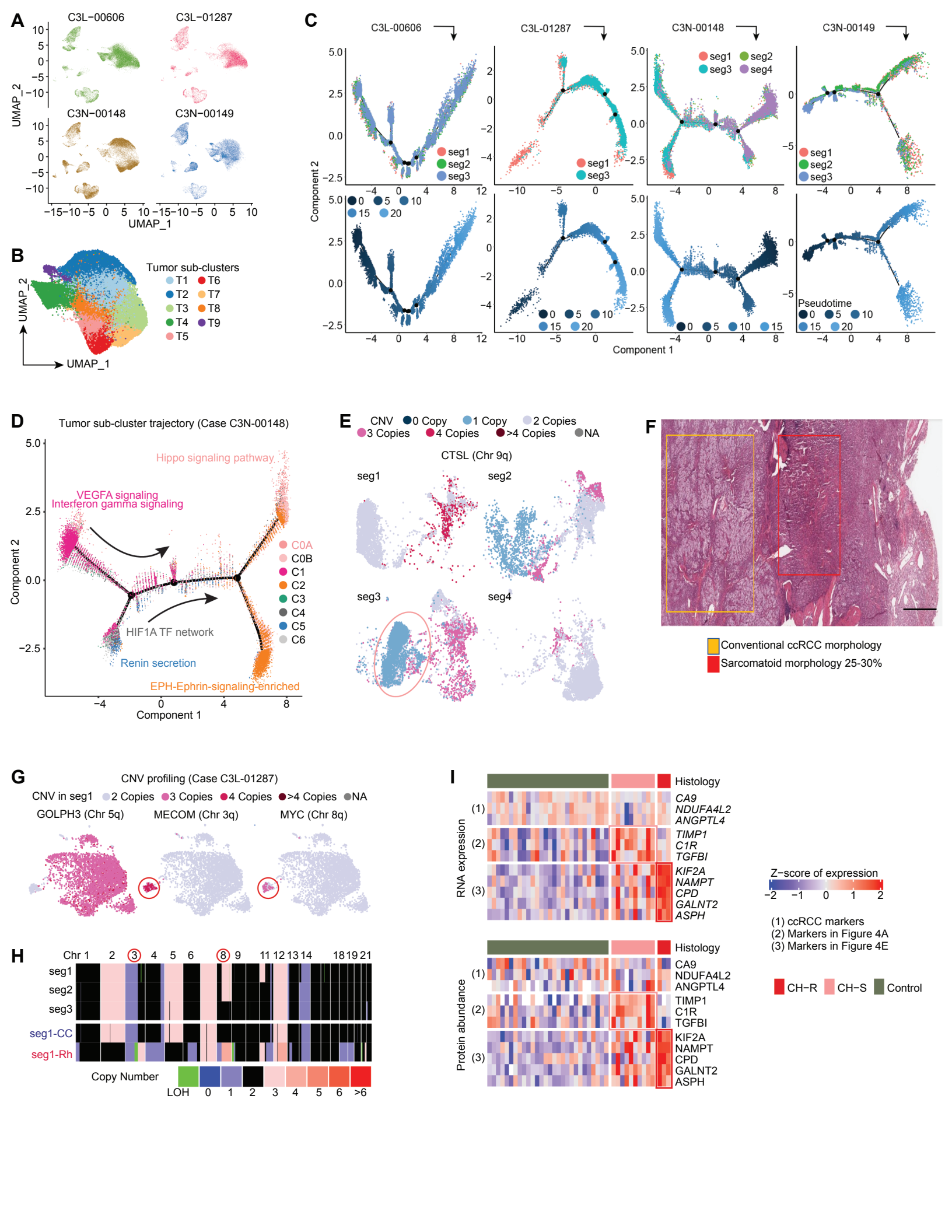
A
C3L−00606
C3L−01287
C3N−00148
C3N−00149
UMAP_2
UMAP_1
B
Tumor sub-clusters
T1
T2
T3
T4
T5
T6
T7
T8
T9
C
C3L-00606
C3L-01287
C3N-00148
C3N-00149
seg1
seg2
seg3
seg4
Pseudotime
Component 2
Component 1
D
Tumor sub-cluster trajectory (Case C3N-00148)
Hippo signaling pathway
VEGFA signaling
Interferon gamma signaling
HIF1A TF network
Renin secretion
EPH-Ephrin-signaling-enriched
C0A
C0B
C1
C2
C3
C4
C5
C6
Component 2
Component 1
E
CNV 0 Copy 1 Copy 2 Copies 3 Copies 4 Copies >4 Copies NA
CTSL (Chr 9q)
seg1
seg2
seg3
seg4
F
Conventional ccRCC morphology
Sarcomatoid morphology 25-30%
G
CNV profiling (Case C3L-01287)
CNV in seg1 2 Copies 3 Copies 4 Copies >4 Copies NA
GOLPH3 (Chr 5q)
MECOM (Chr 3q)
MYC (Chr 8q)
H
Chr 1 2 3 4 5 6 8 9 11 12 13 14 18 19 21
seg1
seg2
seg3
seg1-CC
seg1-Rh
Copy Number
LOH 0 1 2 3 4 5 6 >6
I
Histology
RNA expression
(1)
CA9
NDUFA4L2
ANGPTL4
(2)
TIMP1
C1R
TGFBI
(3)
KIF2A
NAMPT
CPD
GALNT2
ASPH
Protein abundance
Z−score of expression
(1) ccRCC markers
(2) Markers in Figure 4A
(3) Markers in Figure 4E
CH−R
CH−S
Control

Figure S3. Single-nuclei RNA-seq analysis identified sarcomatoid and rhabdoid expression signatures, related to Figures 3-4.

A) The UMAP dimensionality reduction plot displays 10 different cell types (based on biomarker expression and colored accordingly) identified from 104,654 nuclei (with anchoring process) split by cases.

B) The main tumor cluster in Figure S3A includes 9 tumor sub-clusters being enriched in different cases colored by different colors.

C) Trajectory analysis of the four cases is shown and colored by segment ID and predicted pseudotime on the first and second rows, respectively.

D) Tumor sub-cluster trajectory obtained from pseudotime gene expression analysis of case C3N-00148 that shows the relationship among the various tumor sub-clusters.

E) CNV mapping to UMAP shows that segment-3-enriched sub-clusters (C3N-00148) were featured with CNV events including chr9q loss. In these clusters, we also detected 9p (e.g., JAK2) and 13 loss (e.g., RB1).

F) H&E image of the selected region of C3N-00148 segment-3 showing distinct sarcomatoid differentiation and spindle cell proliferation (~25-30%, right side box) juxtaposed to a region with clear cell morphology (left box). Scale bar = 300 microns.

G) Inferred copy number variation (CNV) of select chromosomes mapped to UMAP shows that sub-cluster C0 was characterized by 8q and 3q gains while 5q gain was prevalent in other tumor clusters.

H) Copy number characterization using WES of macro-dissection confirmed the distinct CNV features in the clear cell area (seg1-CC) and rhabdoid area (seg1-Rh).

I) Heatmaps indicate the expression profiles of candidate feature-associated markers (e.g., sarcomatoid, rhabdoid) at the bulk RNA and protein levels.

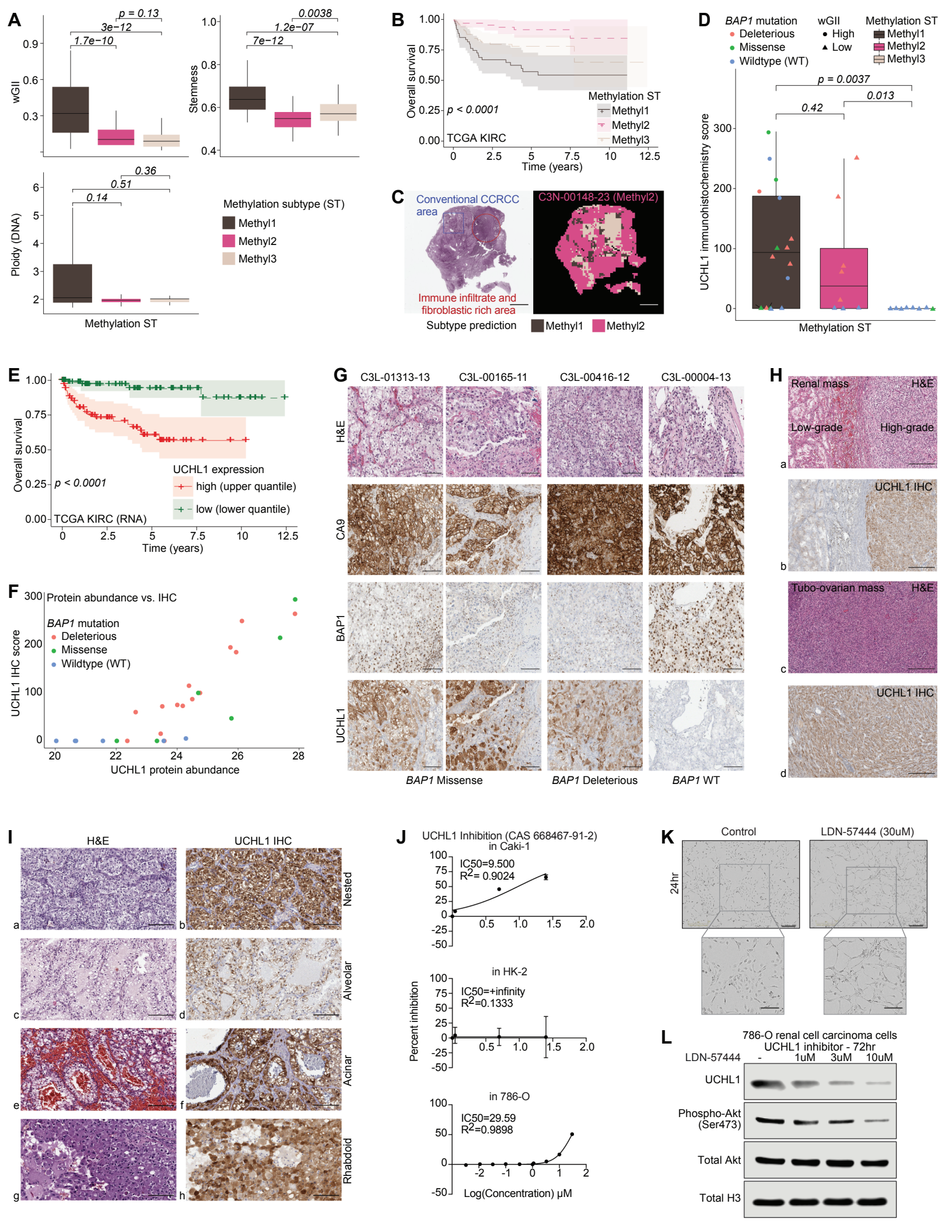
A
p = 0.13
3e−12
1.7e−10
wGII
0.0038
1.2e−07
7e−12
Stemness
0.36
0.51
0.14
Ploidy (DNA)
Methylation ST
Methylation subtype (ST)
Methyl1
Methyl2
Methyl3
B
Overall survival
p < 0.0001
TCGA KIRC
Methylation ST
Methyl1
Methyl2
Methyl3
Time (years)
C
Conventional CCRCC area
C3N-00148-23 (Methyl2)
Immune infiltrate and fibroblastic rich area
Subtype prediction
Methyl1
Methyl2
D
BAP1 mutation
Deleterious
Missense
Wildtype (WT)
wGII
High
Low
Methylation ST
Methyl1
Methyl2
Methyl3
p = 0.0037
0.013
0.42
UCHL1 immunohistochemistry score
Methylation ST
E
Overall survival
p < 0.0001
UCHL1 expression
high (upper quantile)
low (lower quantile)
TCGA KIRC (RNA)
Time (years)
F
Protein abundance vs. IHC
BAP1 mutation
Deleterious
Missense
Wildtype (WT)
UCHL1 IHC score
UCHL1 protein abundance
G
C3L-01313-13
C3L-00165-11
C3L-00416-12
C3L-00004-13
H&E
CA9
BAP1
UCHL1
BAP1 Missense
BAP1 Deleterious
BAP1 WT
H
Renal mass
H&E
Low-grade
High-grade
a
UCHL1 IHC
b
Tubo-ovarian mass
H&E
c
UCHL1 IHC
d
I
H&E
UCHL1 IHC
a
b
Nested
c
d
Alveolar
e
f
Acinar
g
h
Rhabdoid
J
UCHL1 Inhibition (CAS 668467-91-2)
in Caki-1
IC50=9.500
R2= 0.9024
in HK-2
IC50=+infinity
R2=0.1333
Percent inhibition
in 786-O
IC50=29.59
R2=0.9898
Log(Concentration) μM
K
Control
LDN-57444 (30uM)
24hr
L
786-O renal cell carcinoma cells
UCHL1 inhibitor - 72hr
LDN-57444
-
1uM
3uM
10uM
UCHL1
Phospho-Akt (Ser473)
Total Akt
Total H3

Figure S4. Methylation subtype associated with *BAP1* mutations and poor survival, related to Figure 5.

A) Box plots present the distributions of ploidy, wGII score, and stemness score among the methylation subtypes. Significant associations between Methyl1 and wGII, ploidy can be observed. Wilcoxon signed-rank test p is calculated. Boxes represent the interquartile range (IQR, e.g., median indicated by solid line in box, 0.25 and 0.75 quantiles) and whiskers represent the largest and smallest values within 1.5 x IQR range.

B) Kaplan Meier plot indicates the association between overall survival and the three methylation subtypes in TCGA clear cell RCC KIRC cohort. The Methyl1 subtype is significantly associated with poor survival. Log-rank test $p < 0.0001$.

C) Panoptes-based multi-resolution neural network models were trained to predict methylation subtypes based on H&E image. C3N-00148 was classified as Methyl2 which has classic ccRCC histology with marked trabecular change and immune-rich area. Scale bar = 300 microns.

D) The distribution of UCHL1 immunohistochemistry score among methylation subtypes represented by boxplot, and annotated by wGII category and *BAP1* mutation status. Wilcoxon signed-rank test p is calculated. Boxes represent the interquartile range (IQR, e.g., median indicated by solid line in box, 0.25 and 0.75 quantiles) and whiskers represent the largest and smallest values within 1.5 x IQR range.

E) Kaplan Meier plot indicates the association between overall survival and UCHL1 expression in TCGA KIRC cohort. High UCHL1 expression (upper quartile of the cohort) is significantly associated with poor survival. Log-rank test $p < 0.0001$.

F) High correlation between quantified UCHL1 protein abundance versus UCHL1 IHC score is represented by scatter plot. *BAP1* mutation type (deleterious: red, missense: green) and status (wild-type- blue, mutant- red, or green) of the evaluated tumors are indicated.

G) Representative H&E and immunohistochemistry (IHC) images from CAIX, BAP1, UCHL1 IHC validations performed on *BAP1* wild-type and mutated tumors. UCHL1 is overexpressed in most *BAP1* mutated tumors while BAP1 is variably downregulated in *BAP1* mutated tumors. CAIX positivity in all cases as to validate ccRCC cases. Scale bar = 3mm.

H) Characterization of UCHL1 in a patient with primary renal mass (positive UCHL1 expression, stronger in higher grade than lower grade tumor area) (a, b). High and uniform UCHL1 expression in metastatic sarcomatoid differentiated ccRCC tubo-ovarian mass in the same patient (c, d). Scale bar = 200 microns.

I) Strong homogeneous expression of UCHL1 in primary tumors of four different clinically aggressive patients (who developed metastasis) despite varying morphological patterns- conventional nested (a, b), alveolar (c, d), acinar (e, f), and rhabdoid (g, h). Scale bar = 200 microns.

J) Plots indicate the half maximal inhibitory concentration (IC50) of UCHL1 inhibition (CAS 668467-91-2) in Caki-1, HK-2, and 786-O, respectively. R^2 is the square of the correlation.

K) Morphology of Control and CAS 668467-91-2 (30uM, 24hr) treated 786-O renal cancer cells. Scale bars = 300 microns (top), and 200 microns (bottom).

L) Impact of UCHL-1 inhibition on Akt signaling in 786-O renal cancer cells evaluated by Western blot analysis.

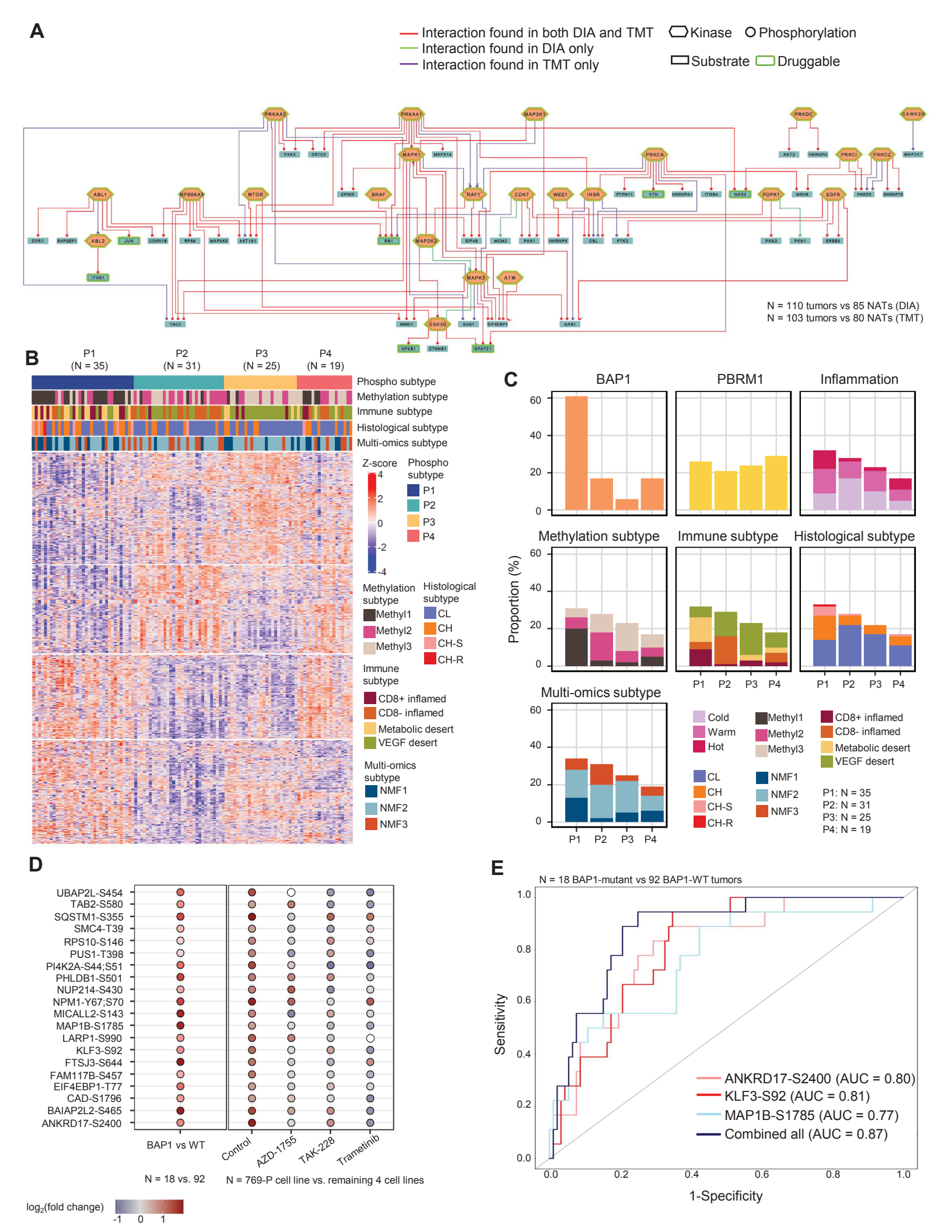
A
Interaction found in both DIA and TMT
Interaction found in DIA only
Interaction found in TMT only
Kinase
Phosphorylation
Substrate
Druggable
N = 110 tumors vs 85 NATs (DIA)
N = 103 tumors vs 80 NATs (TMT)
B
P1 (N = 35)
P2 (N = 31)
P3 (N = 25)
P4 (N = 19)
Phospho subtype
Methylation subtype
Immune subtype
Histological subtype
Multi-omics subtype
Z-score
Methylation subtype
Methyl1
Methyl2
Methyl3
Histological subtype
CL
CH
CH-S
CH-R
Immune subtype
CD8+ inflamed
CD8- inflamed
Metabolic desert
VEGF desert
Multi-omics subtype
NMF1
NMF2
NMF3
C
BAP1
PBRM1
Inflammation
Methylation subtype
Immune subtype
Histological subtype
Multi-omics subtype
Proportion (%)
Cold
Warm
Hot
P1: N = 35
P2: N = 31
P3: N = 25
P4: N = 19
D
UBAP2L-S454
TAB2-S580
SQSTM1-S355
SMC4-T39
RPS10-S146
PUS1-T398
PI4K2A-S44;S51
PHLDB1-S501
NUP214-S430
NPM1-Y67;S70
MICALL2-S143
MAP1B-S1785
LARP1-S990
KLF3-S92
FTSJ3-S644
FAM117B-S457
EIF4EBP1-T77
CAD-S1796
BAIAP2L2-S465
ANKRD17-S2400
BAP1 vs WT
Control
AZD-1755
TAK-228
Trametinib
N = 18 vs. 92
N = 769-P cell line vs. remaining 4 cell lines
log2(fold change)
E
N = 18 BAP1-mutant vs 92 BAP1-WT tumors
Sensitivity
1-Specificity
ANKRD17-S2400 (AUC = 0.80)
KLF3-S92 (AUC = 0.81)
MAP1B-S1785 (AUC = 0.77)
Combined all (AUC = 0.87)

Figure S5. Phosphoproteomic analysis, related to Figure 6.

A) An expanded view of the phospho-signaling network.

B) Heatmap showing K-means clustering results of the phosphoproteomic features among the phosphoproteomic groups.

C) Stacked bar plots highlight the association between select important ccRCC disease variables and the different phosphoproteomic groups.

D) Phosphorylation events upregulated in *BAP1* mutant versus *BAP1* WT tumors comparison as revealed by DIA-based profiling in the tissue cohort and the status of those sites upon various treatments in RCC cell lines.

E) ROC analysis of significantly changed phosphorylation events in *BAP1* mutant and WT tumors.

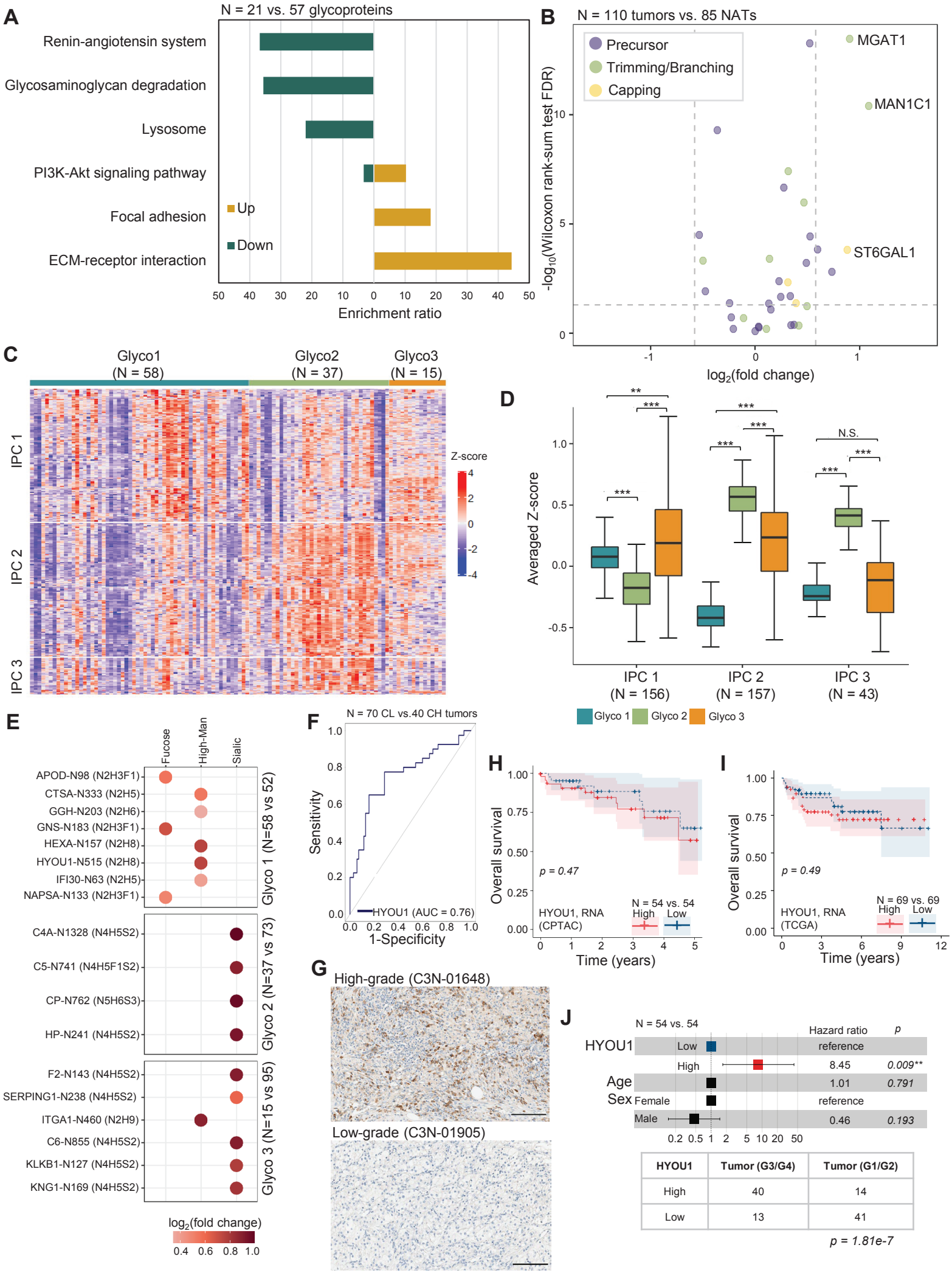
A
N = 21 vs. 57 glycoproteins
Renin-angiotensin system
Glycosaminoglycan degradation
Lysosome
PI3K-Akt signaling pathway
Focal adhesion
ECM-receptor interaction
Up
Down
Enrichment ratio
B
N = 110 tumors vs. 85 NATs
Precursor
Trimming/Branching
Capping
MGAT1
MAN1C1
ST6GAL1
-log10(Wilcoxon rank-sum test FDR)
log2(fold change)
C
Glyco1 (N = 58)
Glyco2 (N = 37)
Glyco3 (N = 15)
IPC 1
IPC 2
IPC 3
Z-score
D
Averaged Z-score
N.S.
IPC 1 (N = 156)
IPC 2 (N = 157)
IPC 3 (N = 43)
Glyco 1
Glyco 2
Glyco 3
E
Fucose
High-Man
Sialic
APOD-N98 (N2H3F1)
CTSA-N333 (N2H5)
GGH-N203 (N2H6)
GNS-N183 (N2H3F1)
HEXA-N157 (N2H8)
HYOU1-N515 (N2H8)
IFI30-N63 (N2H5)
NAPSA-N133 (N2H3F1)
C4A-N1328 (N4H5S2)
C5-N741 (N4H5F1S2)
CP-N762 (N5H6S3)
HP-N241 (N4H5S2)
F2-N143 (N4H5S2)
SERPING1-N238 (N4H5S2)
ITGA1-N460 (N2H9)
C6-N855 (N4H5S2)
KLKB1-N127 (N4H5S2)
KNG1-N169 (N4H5S2)
Glyco 1 (N=58 vs 52)
Glyco 2 (N=37 vs 73)
Glyco 3 (N=15 vs 95)
log2(fold change)
F
N = 70 CL vs.40 CH tumors
Sensitivity
1-Specificity
HYOU1 (AUC = 0.76)
G
High-grade (C3N-01648)
Low-grade (C3N-01905)
H
Overall survival
p = 0.47
HYOU1, RNA (CPTAC)
N = 54 vs. 54
High
Low
Time (years)
I
Overall survival
p = 0.49
HYOU1, RNA (TCGA)
N = 69 vs. 69
High
Low
Time (years)
J
N = 54 vs. 54
Hazard ratio
p
HYOU1
Low
reference
High
8.45
0.009**
Age
1.01
0.791
Sex
Female
reference
Male
0.46
0.193
HYOU1 | Tumor (G3/G4) | Tumor (G1/G2)
High | 40 | 14
Low | 13 | 41
p = 1.81e-7

Figure S6. Alteration of protein glycosylation specific to ccRCC and high-grade ccRCC, related to Figure 7.

A) Significant enriched KEGG pathways using the glycoproteins that exhibit differential intact glycolpeptide expression in tumors compared to NATs. All the enriched pathways had FDR < 0.05.

B) Volcano plot depicts the differentially expressed glycosylation enzymes (n = 35) at the global protein level. Five glycosylation enzymes with >1.5-fold increase (FDR <0.05) in tumors relative to NATs.

C) K-means clustering of the glycoproteomic features in three glycoproteomic subtypes for tumors. Three intact glycopeptide clusters (IPC) were discriminated (IPC1-3).

D) Distribution of each glycoproteomic subtype in association with IPCs shown as boxplots. The outline of the box denotes the interquartile range, the solid line in the box indicates the median, and the whiskers outside of the box extend to the minimum and maximum “averaged Z-score”. Wilcoxon signed-rank test FDR is calculated. N.S. $p \geq 0.05$, * $p < 0.05$, ** $p < 0.01$, *** $p < 0.001$.

E) Bubble plots represent upregulated intact glycopeptides in association with the Glyco subtypes.

F) Performance of HYOU1 for differentiating low-grade and high-grade tumors.

G) Immunochemistry staining of HYOU1 protein expression in high-grade (C3N-01648) versus low-grade (C3N-01905) tumor. Scale bar = 200 microns.

H) Kaplan Meier plot compares HYOU1 between High (upper quartile) and Low (lower quartile) groups at the RNA level in the CPTAC cohort. Log-rank test p is 0.47.

I) Kaplan Meier plot compares HYOU1 between High (upper quartile) and Low (lower quartile) groups at the RNA level in the TCGA cohort. Log-rank test p is 0.49.

J) Forest plot for Cox Proportional Hazards Model adjusting by age and sex (comparing HYOU1 high and low at the protein level in the CPTAC cohort). The hazard ratio of high group is 8.45 from Cox model ($p = 0.009$). Whiskers represent + / - 95% confidence intervals of the hazard ratios. Fisher's exact test result indicates the association between tumor grade and HYOU1 protein abundance ($p = 1.81e-7$).

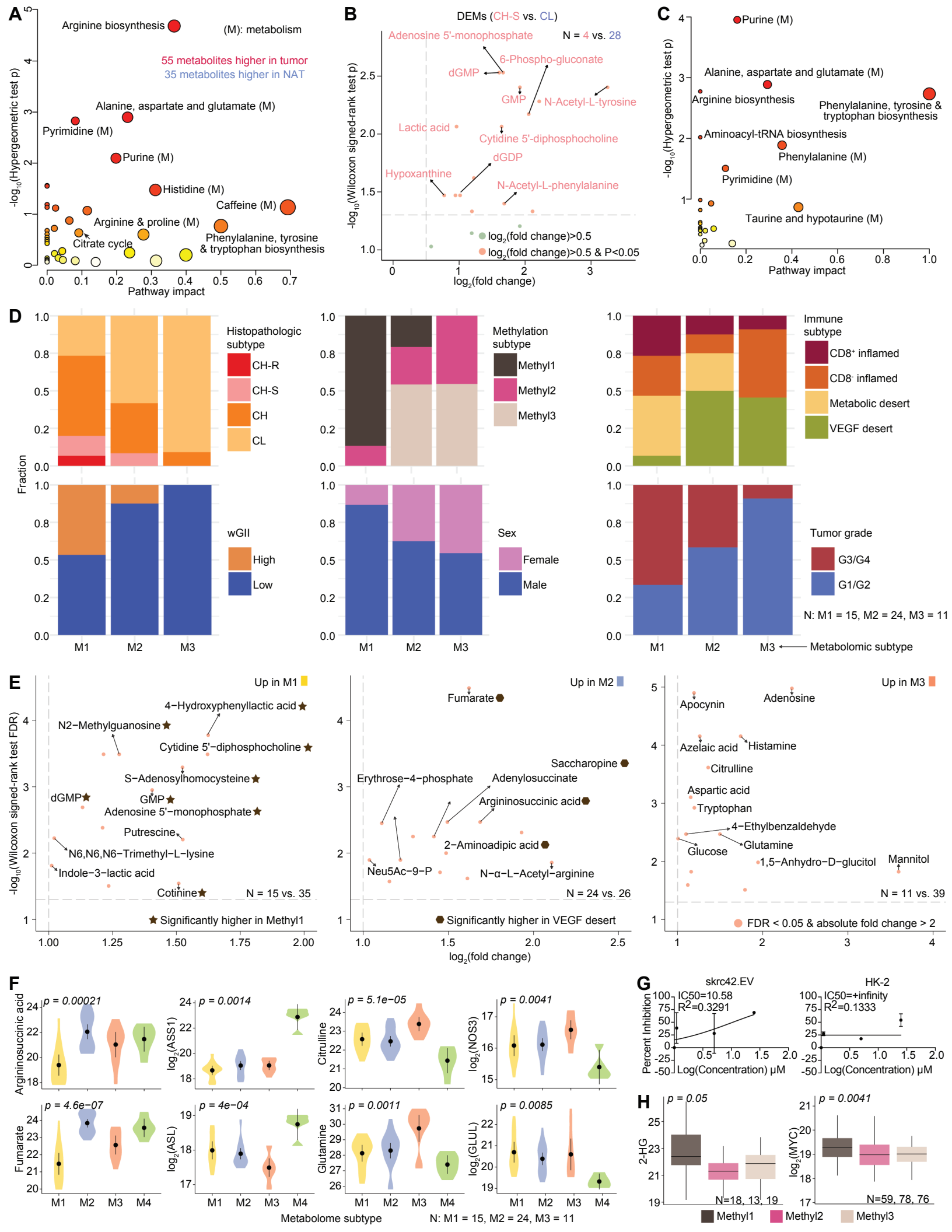
A
Arginine biosynthesis
(M): metabolism
55 metabolites higher in tumor
35 metabolites higher in NAT
Alanine, aspartate and glutamate (M)
Pyrimidine (M)
Purine (M)
Histidine (M)
Caffeine (M)
Arginine & proline (M)
Citrate cycle
Phenylalanine, tyrosine & tryptophan biosynthesis
-log10(Hypergeometric test p)
Pathway impact
B
DEMs (CH-S vs. CL)
N = 4 vs. 28
Adenosine 5'-monophosphate
6-Phospho-gluconate
dGMP
GMP
N-Acetyl-L-tyrosine
Lactic acid
Cytidine 5'-diphosphocholine
dGDP
Hypoxanthine
N-Acetyl-L-phenylalanine
log2(fold change)>0.5
log2(fold change)>0.5 & P<0.05
-log10(Wilcoxon signed-rank test p)
log2(fold change)
C
Purine (M)
Alanine, aspartate and glutamate (M)
Arginine biosynthesis
Phenylalanine, tyrosine & tryptophan biosynthesis
Aminoacyl-tRNA biosynthesis
Phenylalanine (M)
Pyrimidine (M)
Taurine and hypotaurine (M)
-log10(Hypergeometric test p)
Pathway impact
D
Fraction
Histopathologic subtype
CH-R
CH-S
CH
CL
Methylation subtype
Methyl1
Methyl2
Methyl3
Immune subtype
CD8+ inflamed
CD8- inflamed
Metabolic desert
VEGF desert
wGII
High
Low
Sex
Female
Male
Tumor grade
G3/G4
G1/G2
N: M1 = 15, M2 = 24, M3 = 11
M1
M2
M3
Metabolomic subtype
E
Up in M1
4−Hydroxyphenyllactic acid
N2−Methylguanosine
Cytidine 5'−diphosphocholine
S−Adenosylhomocysteine
dGMP
GMP
Adenosine 5'−monophosphate
Putrescine
N6,N6,N6−Trimethyl−L−lysine
Indole−3−lactic acid
Cotinine
N = 15 vs. 35
Significantly higher in Methyl1
Up in M2
Fumarate
Saccharopine
Erythrose−4−phosphate
Adenylosuccinate
Argininosuccinic acid
2−Aminoadipic acid
Neu5Ac−9−P
N−α−L−Acetyl−arginine
N = 24 vs. 26
Significantly higher in VEGF desert
Up in M3
Apocynin
Adenosine
Azelaic acid
Histamine
Citrulline
Aspartic acid
Tryptophan
4−Ethylbenzaldehyde
Glutamine
Glucose
1,5−Anhydro−D−glucitol
Mannitol
N = 11 vs. 39
FDR < 0.05 & absolute fold change > 2
-log10(Wilcoxon signed-rank test FDR)
log2(fold change)
F
Argininosuccinic acid
p = 0.00021
log2(ASS1)
p = 0.0014
Citrulline
p = 5.1e−05
log2(NOS3)
p = 0.0041
Fumarate
p = 4.6e−07
log2(ASL)
p = 4e−04
Glutamine
p = 0.0011
log2(GLUL)
p = 0.0085
M1
M2
M3
M4
Metabolome subtype
N: M1 = 15, M2 = 24, M3 = 11
G
skrc42.EV
IC50=10.58
R2=0.3291
HK-2
IC50=+infinity
R2=0.1333
Percent Inhibition
Log(Concentration) μM
H
p = 0.05
2-HG
N=18, 13, 19
p = 0.0041
log2(MYC)
N=59, 78, 76
Methyl1
Methyl2
Methyl3

Figure S7. Dysregulated metabolism in high-grade ccRCC and low-grade ccRCC, related to Figure 8.

A) Enriched metabolic pathways in the comparison of tumors and NATs.

B) Volcano plot shows the upregulated DEMs in CH-S compared with CL.

C) Enriched metabolic pathways corresponding to CH-S.

D) The distributions of histopathologic, methylation, and immune subtypes, wGII status, sex, and tumor grade among the metabolomic subtypes.

E) Upregulated metabolites associated with each of the methylation subtypes.

F) Expression profiles of key metabolites and enzymes in arginine and proline metabolism. Kruskal-Wallis test p is calculated. Within the violin plots, the dots represent the mean and solid lines indicate the error limit defined by the 95% confidence interval. The violin plot outlines demonstrate the kernel probability.

G) Plots indicate the half maximal inhibitory concentration (IC50) of GLUL inhibition in skrc42.EV and HK-2, respectively. R^2 is the square of the correlation.

H) 2-HG and MYC expressions were significantly higher in Methyl1 (methylation subtype associated with the worse prognosis). Kruskal-Wallis test p is calculated. Boxes represent the interquartile range (IQR, e.g., median, 0.25 and 0.75 quantiles) and whiskers represent the largest and smallest values within 1.5 x IQR range.